Chemical Science

Accepted Manuscript

This article can be cited before page numbers have been issued, to do this please use: Y. Fujii, R. Tatara, Z. T. Gossage and S. Komaba, *Chem. Sci.*, 2025, DOI: 10.1039/D5SC07762A.

ROYAL SOCIETY OF CHEMISTRY

rsc.li/chemical-science

View Article Online
DOI: 10.1039/D5SC07762A

ARTICLE

Revealing the Kinetic Limits of Sodiation and Lithiation at Hard Carbon Using the Diluted Electrode Method

Yuki Fujii,[a] Zachary T. Gossage,[a] Ryoichi Tatara,[a] and Shinichi Komaba*[a]

Received 00th January 20xx,
Accepted 00th January 20xx

DOI: 10.1039/x0xx00000x

Electrochemical sodium- and lithium-insertion into hard carbon (HC) relies on two main reactions: adsorption/intercalation and pore-filling. The rates of these two reactions are key to attaining high power densities and fast charging in batteries, but distinguishing the rate-limitations can be challenging due to their overlap and issues with Na^+ and Li^+ transport in conventional composite electrodes. Herein, we focus on the usage of the diluted electrode method to better evaluate the kinetics of electrochemical sodiation and lithiation at HC. Through galvanostatic charge/discharge testing, cyclic voltammetry and potential step analysis performed on diluted HC-electrodes in aprotic Na cells, we confirm that the sodium-insertion rate into HC is faster than lithium-insertion when we consider both adsorption/intercalation and pore-filling reactions. The apparent ion diffusion coefficients, D_{app}, are on the order of 10^{-10} –10^{-11} and 10^{-10} –10^{-12} cm^2 s^{-1} for sodium- and lithium-insertion, respectively. Furthermore, sodiation into diluted HC-electrode showed comparable rate-capability and D_{app} to lithium intercalation at diluted graphite-electrodes. In addition, we evaluated the temperature dependence using potential-step and electrochemical impedance methods, finding that activation energies, E_a, were ~55 and ~65 kJ mol^{-1} for sodiation and lithiation, respectively. We find reactions in the solid-state, i.e., nucleation of pseudo-metallic clusters, as well as the charge-transfer at the electrolyte/HC interface can limit the rate-performance in diluted HC-electrodes.

Introduction

Currently, hard carbon (HC) is the most promising candidate for the negative electrode of sodium-ion batteries (SIBs).[1] The structure of HC consists of thousands of turbostratic basic-structural-units combined together to create a network of pseudo-graphitic layers and pores.[2,3] These structures have been essential to attaining high reversible capacities for HCs in SIBs in recent years leading to comparable energy densities to lithium-ion batteries (LIBs) using $LiFePO_4$//graphite.[4,5] The sodiation mechanism has been reported as two main steps including: (1) insertion into the interlayer space of the pseudo-graphitic domains and adsorption onto defect sites above 0.1 V, and (2) pore-filling with Na-Na bonding that produces pseudo-metallic clusters below 0.1 V.[6,3] Likewise, LIBs can also utilize this pore-filling mechanism with HC to attain reversible capacities even beyond graphite (over 500 mAh/g).[2,7,8] Furthermore, HC is well known to provide high-rate capabilities and considered to be fast compared with intercalation chemistry at graphite.[9] However, utilizing the pore-filling mechanism at high rates can be difficult due to closeness of the reaction potential to alkali metal plating,[10] and generally no plateau is observed for the lithium insertion process. We have found that this plateau potential can be controlled to an extent via the synthesis methods.[2,11] While the precise HC structure may impact the rate performance for different alkali ions,[2] there is interest to compare the rate capabilities for single active materials to better understand the relationship between structure and rate performance.

Often, high-rate galvanostatic testing is performed using coin-cells or 3-electrode cells to evaluate the power capability of electrode materials. However, this can underestimate the active material rate capabilities due to concentration overvoltage within the composite electrode during high rate operation,[12,13] where guest-ion depletion or saturation of the electrolyte occurs within the porous electrode. To more effectively evaluate the kinetics of the insertion materials, model electrodes such as single-particle, thin-film or monolith material can be utilized.[14–17] Aside, Ariyoshi et al. proposed the usage of a diluted-electrode method where some of the active material within the composite electrode is exchanged for an electrochemically inactive material, *i.e.* Al_2O_3.[18–22] Under these conditions, the separated active-materials are provided sufficient amounts of nearby ions to reach a high state-of-charge (SOC) or depth-of-discharge (DOD) under high current conditions. [18,19]. This dilute-electrode method can evaluate any type of particle while maintaining the composite electrode structure, including the porosity and binder effects. Recently, our group has been using this method to evaluate HC for SIBs, where fast sodiation rates of ~4 C show reversible capacities of *c.a.* 200 mAh/g, or ~85 % of the capacity at 0.1 C insertion rates.[1,23] This makes the dilute electrode method suitable for a detailed comparison of HC for SIBs and LIBs to better understand the relationship between rate and the energy

[a] Department of Applied Chemistry, Tokyo University of Science, Shinjuku, Tokyo 162-8601, Japan
* Correspondence: komaba@rs.tus.ac.jp
Supplementary Information available: [details of any supplementary information available should be included here]. See DOI: 10.1039/x0xx00000x

View Article Online DOI: 10.1039/D5SC07768A

storage mechanism. These are major interest to understand this relationship,[24] but there have been no studies comparing sodiation and lithiation rates at HC using the dilute electrode method.

In this study, we conduct a variety of electrochemical analyses using the diluted-electrode method to compare the sodium- and lithium-insertion kinetics of a commercial HC. We find unique behavior at low and high galvanostatic charging (reduction) rates attributed to the redox of HC and show our method avoids issues with concentration overvoltage in the composite-electrode. At low rates, both the adsorption/insertion and pore-filling mechanism are observed, while only adsorption and insertion occur at high charging rates. In addition to galvanostatic testing, the diluted HC-electrodes were examined using cyclic voltammetry, potential step chronoamperometry, and electrochemical impedance spectroscopy. Based on these various analyses, the sodiation-rates were determined to be faster than lithiation of this HC, especially for the pore filling mechanism and during operation below room temperature. On the other hand, at very high rates with non-diluted electrodes, lithium tended to maintain a higher capacity, which may be related to the larger adsorption- and insertion-capacities for lithium. Overall, the rate of insertion will be majorly limited by the charge-transfer resistance and solid-state diffusion in HC particles. Therefore, a key point of focus for developing improved HC materials for SIBs and LIBs is to attain faster kinetics of the pore-filling process so that they can be accessed at high charging rates.

Experimental section

Electrode preparation

For preparing the composite electrodes, Carbotron® P (J) (Kureha Battery Materials Japan) was used as the active material. Material characterizations of this HC are shown in the supporting information (**Fig. S1**–**S2**). α-aluminum oxide (Al_2O_3, Wako pure chemical) acted as the dilutant, and sodium polyacrylate (Kishida chemical) was used as the binder. **Table S1** shows mass compositions of diluted HC-electrodes. These powders were mixed at various ratios based on volume, HC : dilutant : binder, of x : 95–x : 5 vol./vol. The volume of HC contained in the electrode, x, is defined as the HC-concentration [vol.%]. The volume of the components were calculated based on true densities of each materials, where Carbotron P (J), Al_2O_3, and sodium polyacrylate are 1.52, 3.97, 1.3 g cm^{-3}, respectively.[25–27] Additionally, single-wall carbon nanotubes (SWCNT, Lamfil®, Kusumoto chemical) were used as the conductive additive. As-received product consisted of deionized water : SWCNT : sodium carboxymethyl cellulose (CMC) in weight ratio of 99 : 0.4 : 0.6. Therefore, 100 µL of this dispersion has a total SWCNT mass of ~0.4 mg. The slurry was casted on aluminum foil (20 µm, Hohsen) or copper foil (18 µm, Hohsen), and dried under the ambient conditions. The dried composite electrodes were cut into 10 mm disks and pressed with a mono-axis pressure of ~250 MPa (Specac) to obtain a thickness of 40–47 µm. The prepared electrodes were dried at 150 °C overnight before cell assembly. The homogeneity of the mixed composite electrode was evaluated using scanning electron microscopy (JSM-IT800SHL, JEOL). Electric conductivity of unpressed/pressed composite electrodes were evaluated by using a resistivity meter Loresta-GX (MCP-T700, Mitsubishi chemical analytech) with PSP probe (RMH112, 1.5 mm pins-distance).

Electrochemical cell

R2032-type coin-cells (Hosen) were assembled using the prepared composite electrode as the working electrode in an Ar-filled glove box. Freshly cut metallic Na (99.9 %, Kanto Chemical) was directly immersed in the electrolyte solution, rolled into a thin sheet, and punched into 14 mm (diameter) disks to use as the counter electrode. 1 mol dm^{-3} $NaPF_6$ in ethylene carbonate and diethyl carbonate (1 : 1 v/v) (battery grade, Kishida Chemical) and a glass fiber filter (GB-100R, ADVANTEC) were used as the electrolyte and separator, respectively. Likewise, Li-cells were prepared in a similar manner using Li metal (99.8 %, Honjo Chemical) and 1 mol dm^{-3} $LiPF_6$ in ethylene carbonate and dimethyl carbonate (1 : 1 v/v) (battery grade, Kishida Chemical) as the counter electrode and electrolyte solution, respectively.

Electrochemical measurements

Galvanostatic charge-discharge was carried out on the coin-cells using a battery cycler (TOSCAT-3100, TOYO system). The initial three cycles were conducted applying 25 mA g^{-1} for charge/discharge at 25 °C. The lower cut-off volage was fixed to

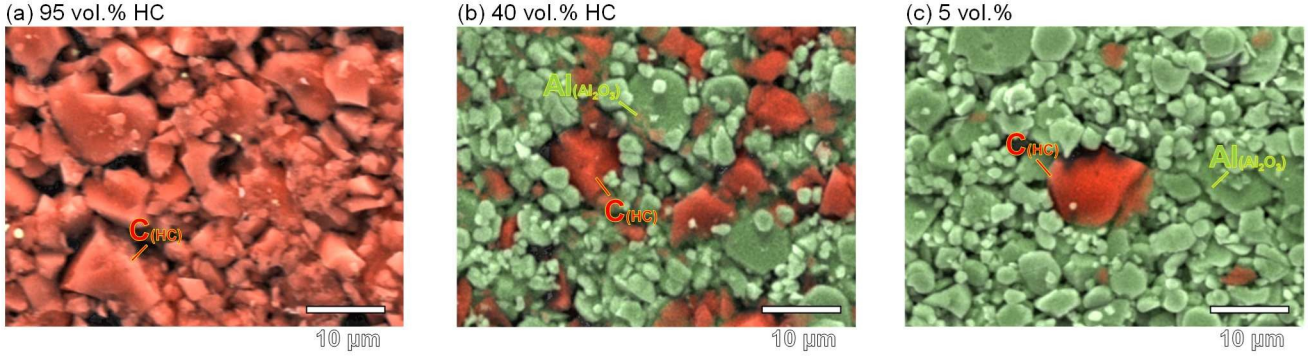

Figure 1. SEM images obtained from top view of composite electrodes containing (a) 95 vol.%, (b) 40 vol.%, and (c) 5 vol.% HC. All images were taken at ×2500 magnification. C in HC and Al in Al_2O_3 are highlighted with red and green, respectively, by energy dispersive X-ray spectroscopy (EDX) mapping.

View Article Online
DOI: 10.1039/D5SC07762A

0.002 V (vs. Na or Li), and the upper cut-off voltage was set to 1.25 V and 1.0 V for Na- and Li-cell, respectively. Between each charge and discharge step, the cell was allowed to rest at open circuit for a period of 5 minutes. After the initial three cycles, the current was systematically increased up to 25,000 mA g^{-1}. A lower current of 5 and 10 mA g^{-1} was employed for tests at 10 °C. For comparative analysis, the reversible capacities were normalized based on the reversible capacity obtained at 25 mA g^{-1}. Using the rate-test data, the apparent diffusion coefficients (D_{app}) were estimated from the slopes in the capacity – current curves based on a spherical diffusion model using OriginPro® (version 2025, OriginLab).

Cyclic voltammetry (CV), potential-step chronoamperometry (PSCA), and electrochemical impedance spectroscopy (EIS) were performed on Na or Li coin-cells (half-cells) with a multi potentiostat (VMP3, BioLogic). During CV, the HC potential was swept between 1.0 V and 0.002 V at a scan rate of 0.02 mV s^{-1} at 25 °C. The scan rate was subsequently increased up to 5 mV s^{-1} to evaluate the scan-rate dependence. PSCA was performed on 5 vol.% HC-electrode using cathodic potential steps from 1.0 V to 0.1 V, and from 0.1 V to 0.002 V, then re-oxidized using potential steps from 0.002 V to 0.12 V and then stepped to 1.0 V. D_{app} were extracted from slopes of linear part in ln (i) – t curves of the chronoamperogram data again based on a spherical diffusion model (calculated in OriginPro® version 2025, OriginLab). EIS was also performed on Na- and Li half-cells by applying ±10 mV amplitude AC voltage at different bias voltages (OCV, 0.5, 0.06, 0.015 V). For the EIS measurements, the cell was reduced galvanostatically using a current of 25 mA g^{-1} followed by a potential hold for 1 hour. Additionally, a 3-electrode cell (TOYO system) and another potentiostat (Squidstat Plus, Admiral Instruments) were partially used for EIS data collection. The fittings of Nyquist plots were performed by Z-Fit in EC-Lab version 11.61 (BioLogic). The temperature dependences of Na-/Li-insertion were evaluated by PSCA and EIS after the high current testing in a range from 10 to 40 °C.

Results and discussions

Electrochemical Characterization

Prior to conducting kinetic analysis of HC for LIBs and SIBs, we prepared and characterized diluted electrodes with varied amounts of diluent and active materials in the composite electrodes. Herein, the diluted electrodes are referred based on the active material content, i.e. 5 vol.% indicates a composite electrode containing 5 vol. % active material, 5 vol. % binder and conductive additive, and 90 vol.% Al_2O_3 both in Na and Li cells. In **Fig. 1** and **Fig. S3**, SEM observation confirms homogeneous dispersion of HC and Al_2O_3 particles. Notably, in 5 vol.% HC-electrode, there was no HC aggregation with the HC particles isolated by surrounding Al_2O_3. We note the electronic conductivity was decreased by dilution with Al_2O_3, but conductivities > 100 S m^{-1} were maintained even in the pressed 5 vol.% HC-electrode with 90 vol.% Al_2O_3. These values are comparable to reported electric conductivity of electrodes for lithium-ion batteries,[28,29] and we ensured a good electronic pathway within the diluted electrodes by using SWCNT. The diluted HC-electrodes were characterized using galvanostatic charge-discharge and CV. As shown in the charge/discharge curves in **Figure 2a** and **2b**, dilution with Al_2O_3 leads to an equivalent loss in the areal (and volumetric) capacities. In all cases, the electrochemical profile is maintained with voltage-slope and voltage-plateau regions, which are typically observed for HCs. Aside, the pure diluted electrodes (95 vol.% Al_2O_3 and 0 vol.% active material) show virtually no reversible capacities in both Na and Li cells. In **Figure 2c** and **2d**, the data have been replotted using gravimetric capacities of the active materials (details shown in **Table S2**). Slow constant-current charging with 25 mA $g_{(HC)}^{-1}$ shows constant values, ~ 240 mAh $g_{(HC)}^{-1}$ and ~300 mAh $g_{(HC)}^{-1}$ in Na- and Li-cell, respectively, for both diluted and conventional electrodes which is consistent with previous reports.[7,23,30,31] For Na (**Fig. 2c**), the reversible capacities were

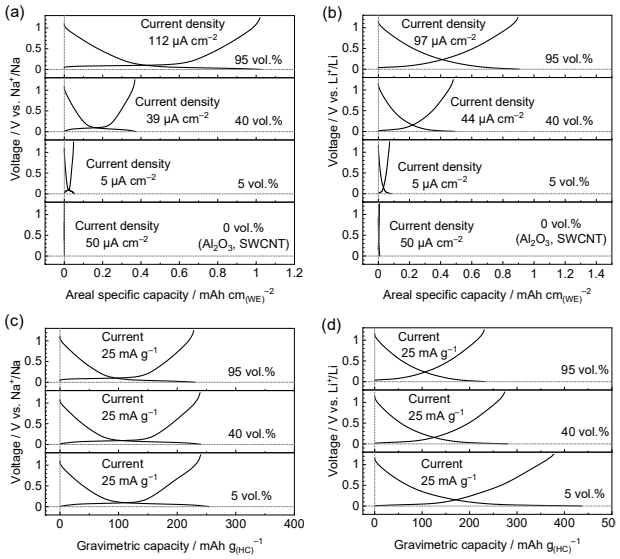

Figure 2. Galvanostatic charge-discharge curves of HC diluted electrodes in Na- and Li-cells. Plotted as (a), (b) areal specific capacities and (c), (d) gravimetric capacities based on the HC mass.

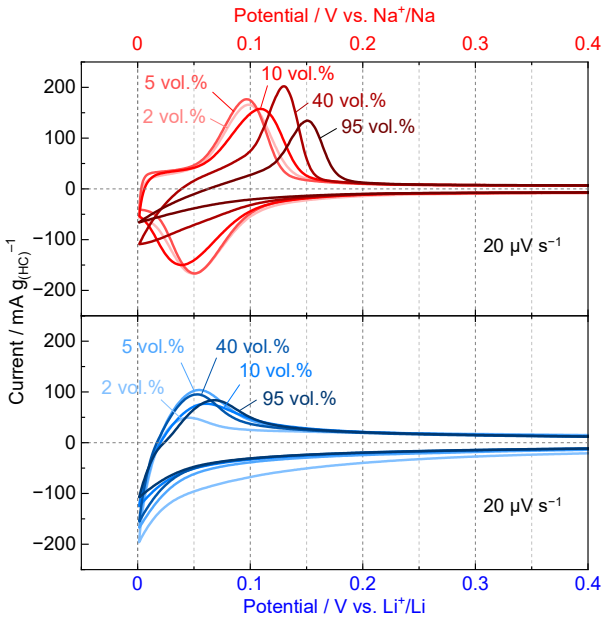

Figure 3. Cyclic voltammogram of (top) Na- and (bottom) Li-cells using various diluted electrodes with a scan rate of 20 μV s^{-1}.

View Article Online DOI: 10.1039/D5SC07763J

similar regardless of the HC-concentration indicating good electronic-conductivity, ionic-conductivity and porosity inside of diluted composite electrodes. Furthermore, there was negligible voltage hysteresis between charge and discharge, indicating negligible ohmic-drop and high reversibility of the reaction.[3] For Li (**Fig. 2d**), the gravimetric capacities increased under dilution, which seems to be related to the pore-filling capacity.[7] In addition, because SWCNT conductive additives can show double layer capacitance, the obtained capacities can be corrected by subtraction of the SWCNT capacity from the total capacity of diluted electrode as shown **Fig. S5** and **Table S2**.

Galvanostatic charge-discharge of cells having extremely diluted-electrode have been reported to suffer from parasitic capacity losses at tiny currents.[22,32] To determine the lower limit of HC-concentration that allows us to evaluate (de)insertion without significant side reaction, Na and Li coin-cells were further investigated using CV in **Fig. 3**. A slow scan rate of 20 μV s^{-1} was used to determine the redox peaks and precisely compare the current of the HC-electrodes. In the Na-cell, the redox peak splitting was continuously suppressed through electrode dilution from 95 to 5 vol.% HC, attaining stable peak currents of ~150 mA g^{-1} for the cathodic- and anodic-peaks at 0.05 V and 0.1 V, respectively. As no further improvements were observed lower than 5 vol.%, this strongly suggests the sodium ion depletion in the interstitial space of the composite electrode is resolved. Therefore. the measured insertion/extraction rates become limited by charge-transfer resistance and solid-state diffusion of sodium in the HC particles.[1,18,23]

In contrast, Li-cells showed only minor improvements in their electrochemical behavior under dilution conditions. The cathodic currents prior to plating ranged from 100 to 200 mA g^{-1} similar to the Na-cells, but no cathodic peak was observed even in the diluted electrode. We believe this is due to the pore filling mechanism occurring at very lower potentials close to $E°$ (Li^+/Li).[7] Still, a small negative shift of the anodic-peak potential and some increase in peak current was observed by electrode dilution. We note this minimal improvement in the Li-cell implies that the lithium insertion/extraction rates of HC are not limited by concentration overvoltage caused by depletion of Li^+ within the composite electrode. Rather, the rates seem to be more dominated by ion transfer at the particle surface or within the HC particles, e.g. solid-state lithium diffusion. In the 2 vol.% HC-electrode in Li-cell, HC redox peaks were deformed by the side-reaction capacity on SWCNT. Therefore, we can conclude that 5 vol.% HC-electrodes are suitable to compare the sodiation and lithiation kinetics of HC.

Rate-capability testing

Next, we evaluated the rate-performance of our diluted electrodes (5 vol.%) and conventional electrodes (95 vol%) in Na and Li cells. As discussed in the introduction, conventional electrodes can show issues with ion supply to the active material at high charging (reduction) rates, while diluted electrodes can alleviate this transport issue to endure higher rates as illustrated in **Fig. 4a**. Such measured rates should be closer to the innate rate of the active material. As shown in the reduction curves for sodiation in **Figure 4b**, low-currents of ≤ 25 mA $g_{(HC)}^{-1}$ showed constant values, ~240 mAh $g_{(HC)}^{-1}$ in Na-cell for both diluted and conventional electrodes. Thereafter, the reduction current was sequentially increased to 1,000 mA g^{-1}, while the oxidation process was carried out using a constant slow rate of 25 mA g^{-1}. As the reduction current increased, the plateau capacity decreased along with polarization attributed to ohmic drop and electrochemical impedance, e.g. the charge-transfer resistance and ion diffusion in the electrolyte, inside HC and at their interface. Likewise, in the Li cell, diluted electrodes showed reduced polarization and could obtain higher capacities at higher rates compared with conventional electrodes.

The compiled results for the Na and Li cells are shown in **Figures 4d** and **4e**, respectively, normalized to the capacities obtained at a slow rate of 25 mA g^{-1}. For Na cells, the undiluted electrode shows a rapid loss in accessible capacity to ~40% at relatively slow rates of ~100 mA $g_{(HC)}^{-1}$ (or ~0.4 C) due to increased polarization and loss of access to the full voltage plateau. At even higher rates, the accessible capacity continued to gradually decrease toward < 10 % at 2,236 mA $g_{(HC)}^{-1}$. On the other hand, 10 vol.% and 5 vol.% HC-electrodes demonstrated improved rate performance that did not show such polarization limitations. They could obtain 80 % and 40 % of the HC capacity at rates of 1,000 and 2,500 mA $g_{(HC)}^{-1}$, respectively. Overall, the rate-capabilities of the diluted electrodes were much higher than undiluted electrodes, suggesting the rate is becoming limited by sodium insertion into HC.[19,23]

The rate performance of lithium insertion was evaluated in the same manner (**Fig. 4e**) and normalized with ~300 mAh $g_{(HC)}^{-1}$ obtained from cycling at 25 mA g^{-1}. The improvements by dilution were much less noteworthy compared to the Na-cell, and the capacities faded to ~60 % before 200 mA g^{-1} even in diluted HC-electrodes. The more negative potential of lower-voltage-plateau attributed to their thermodynamics is one of the factors resulting in less improvement in dilution. However, after this initial loss in capacity, the remaining capacities (> 40%) could be sustained up to 1,000 mA g^{-1} regardless of HC-concentration (**Fig. 4e**). Though the diluted electrodes tended to perform better with sodium, concentrated electrodes with > 40 vol.% HC showed comparable rate-performances to diluted electrode in the Li-cell, especially > 500 mA g^{-1}. This is a bit unexpected considering Na^+ transportation in the electrolyte is faster than Li^+ due to its smaller Stokes radius and less concentration overvoltage for the Na-cell.[33,34] There can be also other factors that impact the final rate performance such as the complex resistance in high HC-concentration as discussed later (Section 3.4). Furthermore, the relatively smaller activation energy correlating to SEI on conventional electrode,[35] and the capacity of the sloping region (above 0.1 V vs. Li^+/Li) for lithiation is relatively large compared with sodiation, and this seems to enable such higher rate capability. We speculate this may be related to the SEI, which are known to be different for Na and Li systems,[36] but also may be influenced by the diluted electrode structure where may homogeneous SEI can be formed on HC particles as same as microelectrodes.[37]

For additional quantification of the insertion kinetics of sodium and lithium into the 5 vol.% HC-electrodes, the apparent

View Article Online
DOI: 10.1039/D5SC07762A

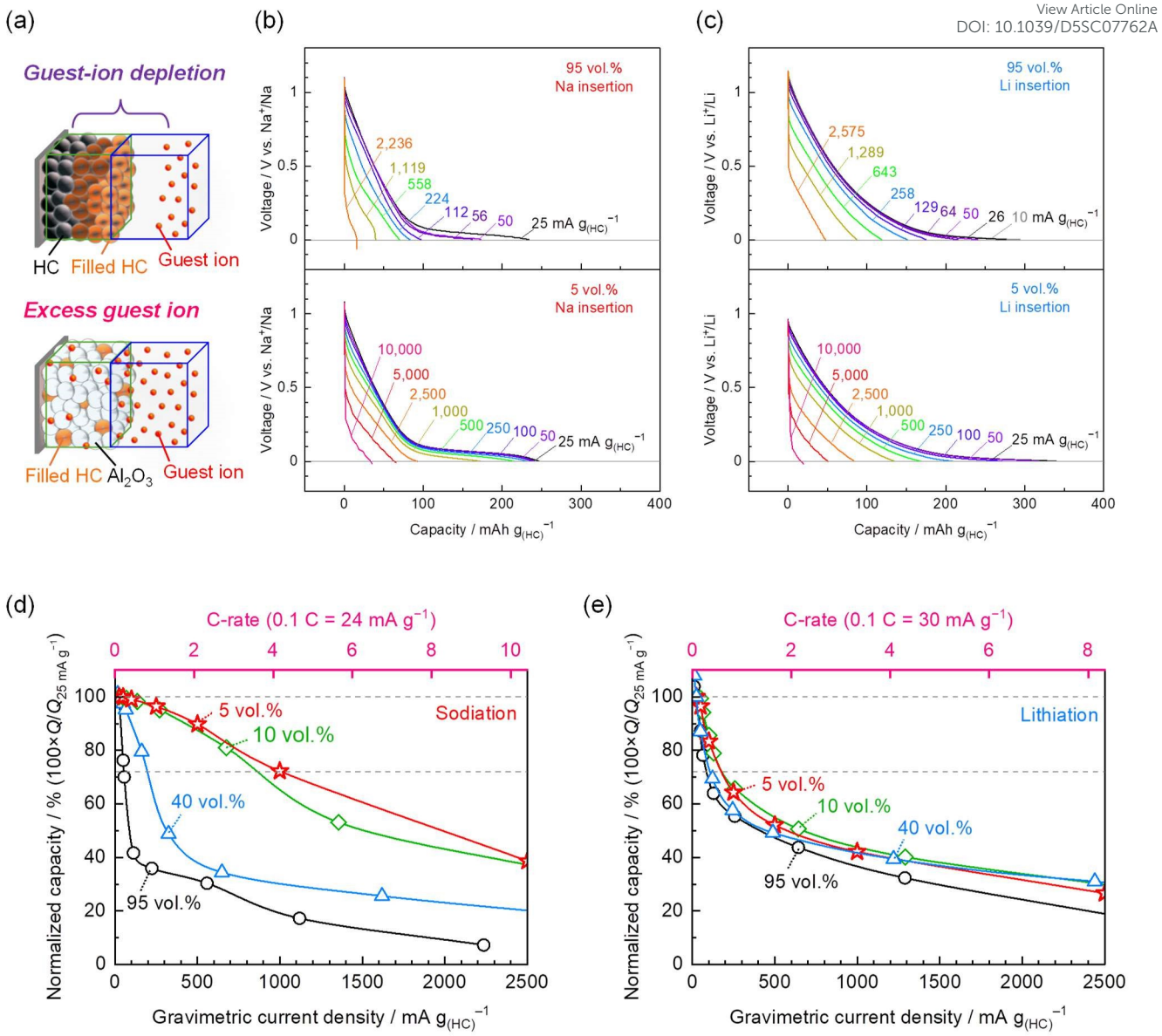

Figure 4. Rate testing at room temperature using electrodes at various HC-concentration. (a) Schematic image of the electrode condition during high-rate reduction. Charge-discharge curves of undiluted and diluted HC-electrode in (b) Na-cells and (c) Li-cells. Rate capabilities of HC electrodes during insertion process for (c) sodiation and (e) lithiation.

diffusion coefficients (D_{app}) were estimated from the rate-capability curves using **Eq. 1**.[20,38,39]

$$Q = \frac{Ca}{3} - \frac{a^2}{15D_{app}} j_m \quad (1)$$

Here we defined Q [mC $g_{(HC)}^{-1}$] as the reversible capacity of HC obtained at each applied current, C [mol dm^{-3}] as the concentration of guest-ion in HC, a [cm] as the particle radius of HC, and j_m [mA $g_{(HC)}^{-1}$] as the current applied. The capacity decrease was proportional to the applied current, and D_{app} was estimated by using only second term of **Eq. 1** and the linear parts of capacity decay (**Fig. S6**).[38] At slow rates involving both slope capacity (adsorption/intercalation) and plateau capacity (pore-filling), D_{app} of the Na-cell (5.7×10^{-11} cm^2 s^{-1}) was found to be faster than the Li-cell (5.6×10^{-12} cm^2 s^{-1}). There is an additional capacity region with higher D_{app} (4.5×10^{-11} cm^2 s^{-1}) in the Li cell, which is corresponding to middle-potential region attributed to the lithium-insertion into narrow interlayer space of the carbon planes.[2] At faster rates which mostly involve adsorption/intercalation, D_{app} for Na and Li are quite similar at 5.8×10^{-10} and 5.1×10^{-10} cm^2 s^{-1}, respectively. The magnitude orders and trends of obtained values are consistent with previous reports of 10^{-10}–10^{-13} cm^2 s^{-1}.[40–42]

The polarization of the charge-discharge curves was further used to evaluate the charge-transfer resistance, R_{ct}, of the cells through Tafel plots. From the galvanostatic charge-discharge curves using 5 vol.% HC-electrode, the cell voltages were extracted at capacities of 25 and 100 mAh g^{-1} during reduction and 100 and 200 mAh g^{-1} during oxidation (**Fig. S7**) to evaluate polarization at slope- and plateau-region, respectively. As shown in **Fig. S8**, these results are plotted as polarization (η) versus the applied current at the HC electrodes. η was defined

View Article Online DOI: 10.1039/D5SC07763A

by subtracting the voltage from (dis)charge curves measured at low currents. We note that the polarization of the counter electrode is negligible in the dilute electrode similar to single-particle measurements,[14,43] so the differences in η can be attributed to alkali-ion insertion/extraction at the HC-electrode. Obtained values of η for sodium insertion were smaller than that of lithium at high rates. Looking at the Tafel plots derived from de-sodiation/de-lithiation (oxidation) at 200 mAh g^{-1}, Na cell showed larger polarization which may be attributed to increased resistivity at low SOC (**Fig. S8a** and right panel). R_{ct} can be estimated from the exchange current densities (j_0) as shown in **Eq. (2)** [14].

$$R_{ct} = \frac{RT}{Fj_0} \quad (2)$$

Here R is the gas constant, T is the temperature, and F is the Faraday constant. j_0 were obtained by extrapolation from the Tafel region in the η–log(j_m) plots of 25 mAh g^{-1} during insertion or 100 mAh g^{-1} and 200 mAh g^{-1} during extraction. Estimated R_{ct} in slope-capacity region at 25 mAh g^{-1} were 105–128 Ω $mg_{(HC)}$ in the Na-cell and 103–114 Ω $mg_{(HC)}$ in the Li-cell, respectively (**Fig. S8a**). Furthermore, the insertion plateau-capacity region at 100 mAh g^{-1} during extraction showed R_{ct} of 70 Ω $mg_{(HC)}$ in the Na-cell and 105 Ω $mg_{(HC)}$ in the Li-cell, respectively (**Fig. S8b**). These results suggest that the exchange current density of Na^+ on sodiated HC can be comparable or slightly higher than Li^+ on lithiated HC, relating to not only the electrochemical process at the electrode/electrolyte interfaces, but also the SOC of HCs.[44,45] Tafel plots deviated from linearity at higher currents, implying the rate-limitation of mass transport in the HC particles.[14] Therefore, the rate-performance as shown in **Fig. 4d–e** can be majorly limited by the charge-transfer resistance.

As an additional comparison, we tested the rate capability of lithium intercalation using natural graphite flakes with the

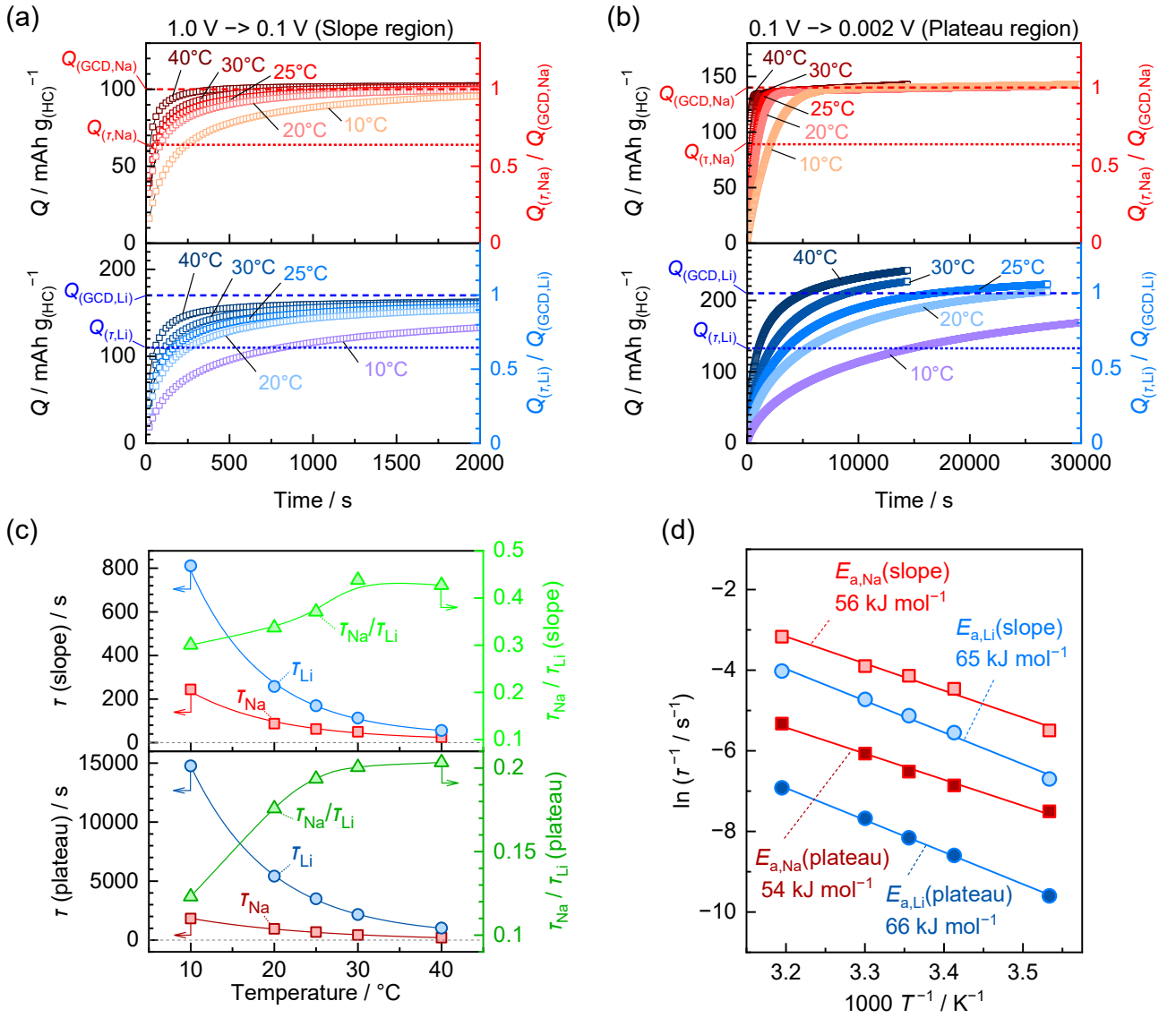

Figure 5. PSCA for sodiation and lithiation of 5 vol.% HC electrodes. Chronocoulograms corresponding to potential steps (a) from 1.0 V to 0.1 V and (b) from 0.1 to 0.002 V in Na- and Li-cells under various temperature. (c) Relationships between temperature and relaxation times of sodiation/lithiation obtained from chronocoulograms, and (d) corresponding Arrhenius plots.

View Article Online
DOI: 10.1039/D5SC07762A

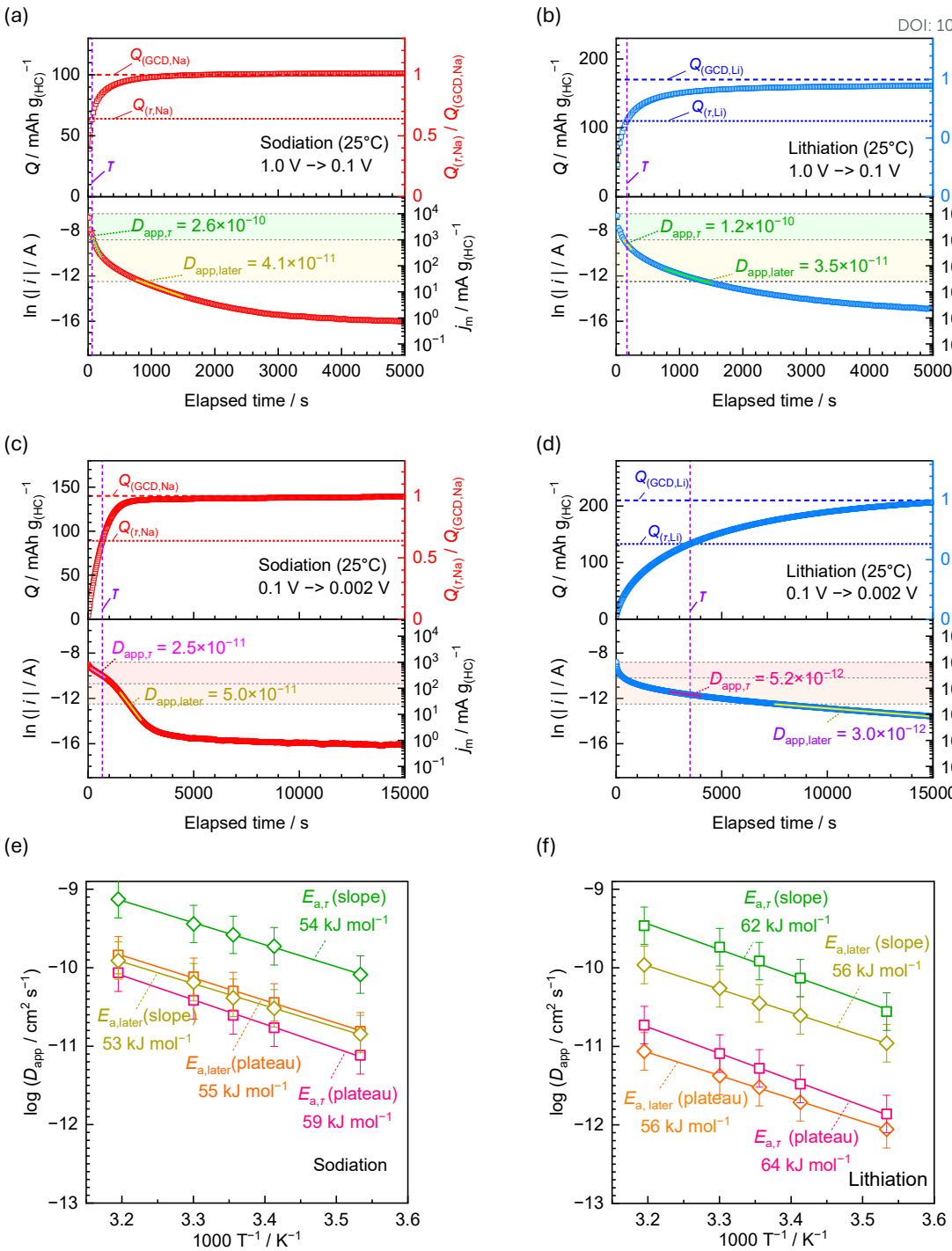

Figure 6. Chronocoulograms and corresponding chronoamperograms of 5 vol.% HC electrodes for the slope region of (a) sodiation and (b) lithiation, and plateau regions for (c) sodiation and (d) lithiation. The values of D_{app} were estimated by applying **Eq. 4** as described in the experimental section. Activation energies $E_{a,\tau}$ and $E_{a,later}$ were estimated from D_{app} vs. T^{-1} plots of $D_{app,\tau}$ and $D_{app,later}$ during (e) sodiation and (f) lithiation, respectively. The error bars of D_{app} values are estimated from standard error of the HC particle size.

diluted-electrode method as shown in **Fig. S9**. Using a 5 vol.% graphite-electrode, where rates are not limited by Li^+ supply, we could obtain 75 % (at 755 mA $g_{(graphite)}^{-1}$) and 41 % (at 1,891 mA $g_{(graphite)}^{-1}$) of the capacity at low lithium-intercalation rates. The evaluated D_{app} based on rate-capability curves using **Eq. S3** in supporting information was 2.8×10^{-10} cm^2 s^{-1}. Overall, this indicates that lithium diffusion coefficient into graphite is lower than the adsorption/intercalation of lithium and sodium at HC. On the other hand, our results also indicate these rates are significantly faster than the pore-filling mechanism, which leaves a point of focus for future research to further enhance the power capabilities of HC for LIBs and SIBs. We have observed similar kinetic advantages for sodium in ether-based electrolytes (**Fig. S10**) using diethylene glycol dimethyl ether

View Article Online
DOI: 10.1039/D5SC07763A

(G2), which is a well-known battery solvent which can form robust and low resistive SEI on negative electrodes.[46,47] The electrolyte, consisting of 1 M NaPF6 in G2, drastically improved the sodiation rate-capability alike to previous reports.[46] The 5 vol.% HC electrodes maintained > 90 % capacity at 2,500 mA g^{-1} (~10 C) in the Na-cell. In comparison, the Li-cell containing 1.5 M lithium bis(fluorosulfonyl)amide dissolved in G2 also showed enhancement in lithiation, but significantly less than the improvements observed with Na-cells. Although detailed kinetic analysis of other electrolytes and the role of the SEI property is currently ongoing in our laboratory, these additional results further reinforce our conclusion that sodium insertion into this HC is intrinsically faster than lithium insertion.

Chronocoulometry and chronoamperometry

Next, we further investigated the kinetics of Na and Li insertion/extraction using potential step chronoamperometry (PSCA) at 5 vol.% electrodes.[22,48] In this case, the potential control can be used to help separate the reactions corresponding to different storage sites by assuming the slope and the plateau regions. **Figure S11a** shows applied potential-steps and resulting chronoamperograms for the Na- and Li-cells. For the initial step from 1.0 V to 0.1 V regarding the slope region, the reduction currents reached to ca. −7.5 A g^{-1} and quickly decayed to 0 A g^{-1}. As the potential was stepped lower to 0.002 V which includes the plateau capacity, smaller currents of ~ −1.0 A g^{-1} were observed (**Fig. S11b**). The Li-cell showed higher current than the Na-cell due to the larger capacity for adsorption/intercalation and electric double layer charging. Chronocoulograms showed good reversibility of capacity for slope and plateau region that are consistent with capacities collected using galvanostatic charge/discharge (See **Fig. S12**).

PSCA was also conducted at various temperatures as shown in **Figure 5a** and **5b**. The data were converted to chronocoulograms for the slope and plateau regions. To compare the reaction rate, the relaxation time (τ) for formation of NaC_x or LiC_x was defined as the time when capacity reached to $Q_{(\tau)}$ that is $1-e^{-1}$ (63.2 %) of the $Q_{(GCD)}$, collected in **Table. S3**. The obtained τ are shown in **Fig. 5c** as a function of temperature. The resulting τ_{Na} and τ_{Li} showed an inverse relationship with temperature (in 40–10 °C) for the slope and plateau regions. Interestingly, the ratio between sodium- and lithium-insertion, τ_{Na}/τ_{Li} were decreased, especially at lower temperatures (**Fig. 5d**). This implies that Na^+ insertion into hard carbon may be able to attain faster charging rates at lower temperatures. As is well known, relaxation time can provide a kinetic constant (k) and activation energy (E_a) as following **Eq. 3** and **Eq. 4**, respectively:

$$\tau = \frac{1}{k} \quad (3)$$

$$E_a = \ln\left(\frac{1}{\tau}\right)/T \quad (4)$$

Figure 5d shows $\ln(\tau^{-1})$ $-T^{-1}$ plot and estimated E_a. We found that E_a for sodium insertion at 56 and 54 kJ mol^{-1} for the slope and plateau region, were lower than lithium insertion at 65 and 66 kJ mol^{-1}.

Under PSCA, we can also evaluate D_{app} expressed by Fick's second law. Here we estimate the D_{app} from linear parts of the $\ln(i)$–t plots using a spherical model as shown in **Eq. 5** assuming 5 vol.% diluted electrodes behave like single-particle electrodes.[48–50] The equation follows as:

$$\ln(i) = \left(-\pi^2 D_{app}/a^2\right)t + \ln\left(2nFAD_{app}\Delta C/a\right) \quad (5)$$

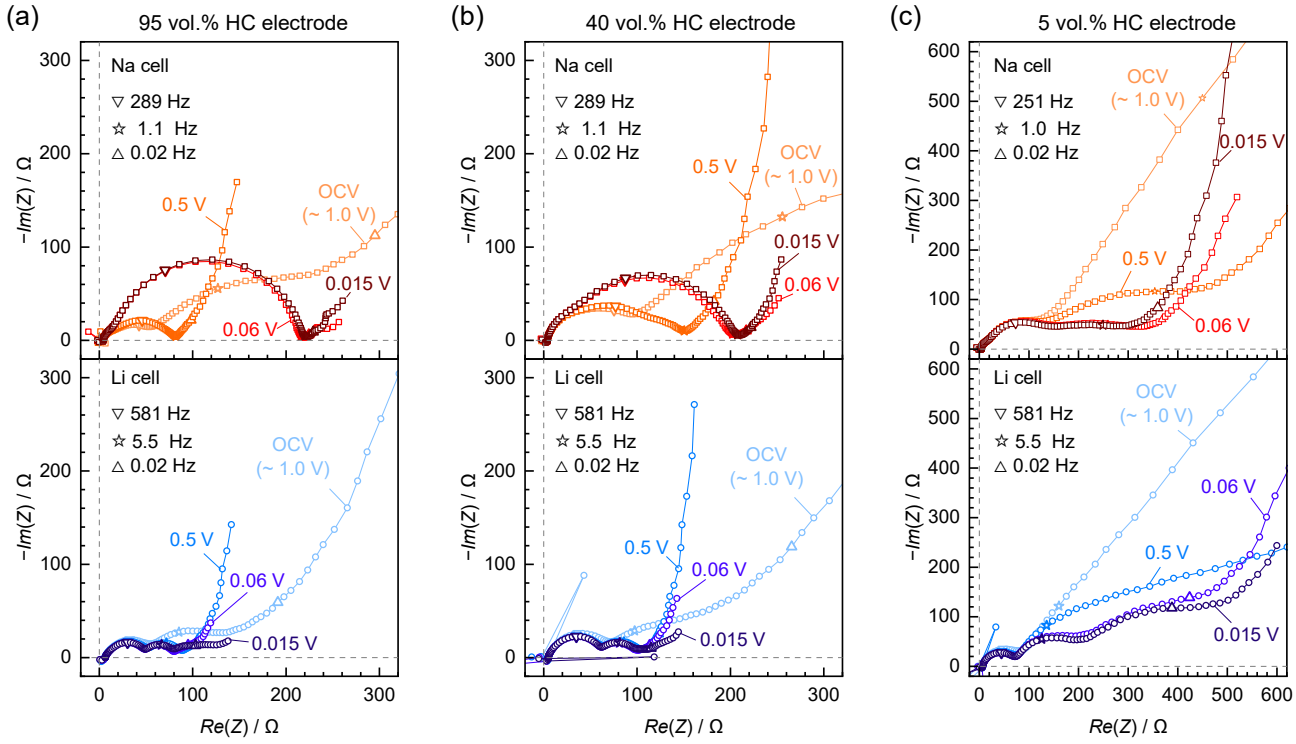

Figure 7. Nyquist plots of electrochemical impedance obtained in 5th cycle of Na- and Li-cell with (a) 95, (b) 40, and (c) 5 vol.% HC electrodes.

View Article Online
DOI: 10.1039/D5SC07763A

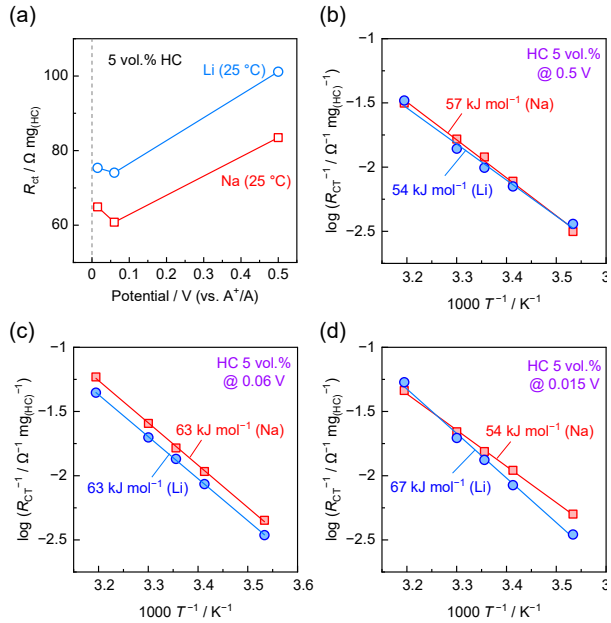

Figure 8. (a) R_{ct} values of 5 vol.% HC electrodes evaluated by fitting of electrochemical impedance spectra obtained after high-current test. log (R_{ct}^{-1}) – T^{-1} plots collected at (b) 0.5 V, (c) 0.06 V, and (d) 0.015 V.

where *a* is the radius of the HC particles, *t* is the elapsed time after the potential step, *n* is the charge of the diffusing species, *F* is Faraday's constant, *A* is the surface area of the particle, and *ΔC* is the concentration change of guest-ion in particles induced by the potential step. Ideally, the applicable time range is often noted as greater than diffusion-characteristic time, $a^2 / \pi^2 D_{app}$, where after obtaining the concentration gradient in diffusion matrix. The most effective advantage of this model is that we can evaluate D_{app} without the second term including surface area and concentration, because the first term allows us to obtain D_{app} from the slope in ln(*i*) – *t* plots. Chronoamperograms obtained from PSCA at 25 °C are shown in **Fig. 6** with their corresponding chronocoulograms. In both Na- and Li-cells, the current associated with the slope region showed a rapid decrease from ln(|*i*|) = −7 to −10 within 500 s and a subsequent slow decay until 3000 s (**Fig. 6a** and **6b**). The obtained $D_{app,\tau}$ values were 2.6×10^{-10} and 1.2×10^{-10} cm^2 s^{-1} at short times for 200 s and 300 s, respectively, which agreed with the results of the rate-capability testing (see **Fig. S6**). This rate decreased to 4.1×10^{-11} and 3.5×10^{-11} cm^2 s^{-1} ($D_{app,later}$) during the following slow decays after 760 s for sodium-/lithium-insertion, respectively.

When applying polarization into the plateau region, as shown in **Fig. 6c** and **6d**, linear parts of ln(*i*)–*t* plots were observed implying solid-state diffusion from insertion and pore-filling.[3,6,7,10] Sodiation maintained high currents >100 mA g^{-1} for 1200 s, followed by a current decay to 1 mA g^{-1} by 3000 s. The former fast current decay partially had smaller values of $a^2 / \pi^2 D_{app}$ that implies a charge-transfer limiting process. We must keep in mind some ambiguity in isolating these different processes, but the obtained $D_{app,\tau}$ and $D_{app,later}$ were 2.5×10^{-11} and 5.0×10^{-11} cm^2 s^{-1}, respectively. This current behavior is similar to the lithium insertion of $Li_{4/3}Ti_{5/3}O_4$ reported by Takami et al.,[15] therefore, we also used a core-shell model for gaining kinetic insight of the plateau region. $D_{app,\tau}$, and $D_{app,later}$ for lithiation were 5.2×10^{-12}, and 3.0×10^{-12} cm^2 s^{-1}, respectively, in good agreement with the rate-capability tests.

The temperature dependence of chronoamperograms and D_{app} were further investigated as shown in **Figs. S13** and **S14**, respectively. The log (D_{app})–T^{-1} plots are shown in **Figs. 6e** and **6f**. Both Na- and Li-cells showed similar results to room temperature measurements with almost the same shape for the chronoamperograms between 10–40 °C. D_{app} for the slope region varied between ~10^{-10}–10^{-11} cm^2 s^{-1} for both sodium- and lithium-insertion. These results agree well with self-diffusion coefficients obtained from positive-muon spin relaxation at ~10^{-10}–10^{-11} cm^2 s^{-1} for NaC_x (HC), LiC_6 (graphite) and LiC_{12} (graphite) in our previous reports.[51,52] On the other hand, the plateau region delivered slower diffusion coefficient in ~10^{-10}–10^{-12} cm^2 s^{-1}, which is consistent with charge/discharge rate testing where the plateau region becomes inaccessible at high rates due to complex kinetic factors, i.e., nucleation of pseudo-metallic clusters. **Figure 6e** and **6f** show corresponding E_a calculated using **Eq. 6**;[53]

$$D_{app} = A \exp\left(\frac{E_a}{k_B T}\right) \quad (6)$$

where *A* is the pre-exponential factor, k_B is the Boltzmann constant, and *T* is the temperature. We found that E_a for sodium insertion at 53–54 and 55–59 kJ mol^{-1} for the slope and plateau regions, and lithium insertion at 56–62 and 56–64 kJ mol^{-1} consistent with E_a obtained from *τ* of chronocoulogram (**Fig. 5d**).

Electrochemical impedance spectroscopy

As a final analysis of these two systems, we focused on EIS as shown in the Nyquist plots for the Na- and Li-cells (**Figure 7**) using 95, 40 and 5 vol% HC-concentration electrodes. The EIS measurements were performed at OCV, 0.5 V, 0.06 V and 0.015 V during the 5th galvanostatic charge/discharge cycle. Aside from the half-cell, we also evaluate the impedance of symmetric cells of Na or Li metal disks as shown in **Fig. S15**. According to the frequency response in the half- and symmetric-cells, the semicircles at higher and lower frequencies are mostly attributed to the counter and the working electrodes, respectively.[54]

Moving from OCV to 0.5V, all cells showed impedance decrease at low frequencies with electrochemical reduction of HC as previously reported.[54,55] Interestingly, cells using electrodes with higher HC-concentration, i.e., 95 and 40 vol.% in **Figs. 7a** and **7b**, showed an increase in resistance was observed at 0.06 V and 0.015 V. Furthermore, expansion of the semicircle between 2,000–1 Hz in the Na cell and an additional semicircle developed between 1–0.01 Hz in the Li cell, regardless of whether there were dilutants. Even in 3-electrode cells using 40 vol.% HC-electrodes (**Fig. S16a** and **S16b**), the increase in impedance was pronounced after reaching potentials corresponding to the plateau region in both Na and Li cells; lower than 0.06 V vs. Na^+/Na and 0.015 V vs. Li^+/Li, respectively. Simultaneously, as shown in magnified Nyquist plots (**Fig. S16c** to **S16d)** and Bode plots (**Fig. S17**), there were apparent

View Article Online
DOI: 10.1039/D5SC07763A

expansions of the higher frequency semicircle at > 100 Hz, that we can attribute to guest-ion transportation in porous structures,[56] contact resistance between particles,[57–59] and inhomogeneities of SOC.[45,60–62] Interestingly, during the extraction process shown in **Figs. S16e–S16h**, the impedance decreased until 0.08 V and then increased again at 0.6 V, especially in the Na-cell. We speculate that the increasing impedance in higher HC-concentration may be caused by an inhomogeneous SOC distribution of the HC particles throughout the composite electrode which occurs due to the guest-ion depletion (**Fig. 4a)** during the insertion process. This drastic guest-ion consumption could be a factor that results in lower rate capabilities of the Na-cell, therefore, it should be considered when designing the high-power HC electrode for optimizing the fast transport of solvated Na^+ in electrolyte.[33,63] On the other hand, using 5 vol.% HC-electrode (**Fig. 7c**) that can suppress the concentration overvoltage in the electrolyte, led to smaller impedance during electrochemical reduction from 0.5 V to 0.06 V. Simultaneously, total impedance becomes larger up to 600 Ω because of low loading of HC. The Na-cell showed an unclear semicircle attributed to HC at frequencies lower than 25 Hz and was difficult to deconvolute to two parallel components with good reproducibility. **Figure S18** and **Figure S19** show the Nyquist plots of cycled electrodes (after high-current testing). We used the equivalent circuit shown in **Fig. S20a** for analysis regarding the wide semicircle located around 1 Hz. A slightly different equivalent circuit, shown in **Fig. S20b**, was applied to the Li-cell to accommodate the larger semicircles located around 5.5 Hz and 0.02 Hz, attributed to HC and side reactions at other components such as SWCNT, respectively. Also to accommodate the absence of capacitive behavior at lower frequencies. **Figure 8** and **Table S4** show evaluated R_{ct} values which were normalized based on the HC mass. The resistance obtained in 25 °C at 0.5 V, 83 Ω $mg_{(HC)}$ in Na cell and 101 Ω $mg_{(HC)}$ in Li cell were consistent with R_{ct} estimated from Tafel plots (See **Fig. S8**). When the electrodes were electrochemically reduced from 0.5 V to 0.06 V, both cells showed a decrease in their R_{ct}, and those values remained nearly constant after further reduction to 0.015 V as reported.[40] Through log $(R_{ct}^{-1}) - T^{-1}$ plots shown in **Fig. 8b–c**, we found that sodiated-HC at the higher SOC (0.06 V and 0.015 V) has smaller R_{ct} compared with lithiated-HC in agreement with our PSCA results (**Fig. 5c**). E_a were extracted from log $(R_{ct}^{-1}) - T^{-1}$ plots using **Eq. 7**:[40]

$$R_{ct}^{-1} = A \exp\left(-\frac{E_a}{RT}\right) \quad (7)$$

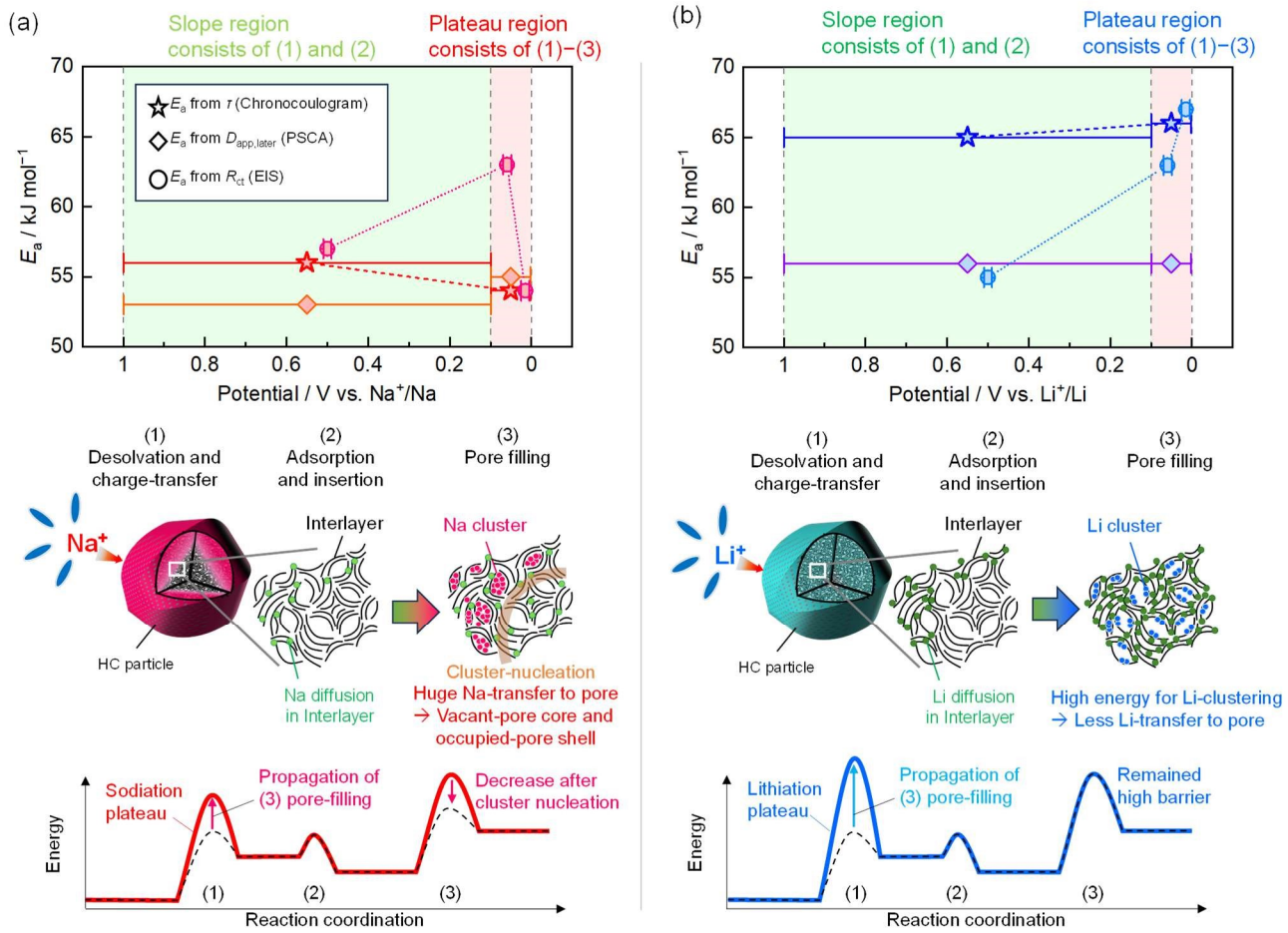

Figure 9. The summarized results of E_a for (a) sodiation and (b) lithiation of HC from our various measurements; E_a during insertion process obtained from τ of chronocoulogram, $D_{app,later}$ estimated from PSCA, and R_{ct} evaluated by EIS.

Here, A is the pre-exponential constant, and R is the universal gas constant. Electrochemical reduction from 0.5 V and 0.06 V increased E_a in the both Na- (57 kJ mol^{-1}) and Li-cells (54 kJ mol^{-1}) to 63 kJ mol^{-1}. However, upon further reduction to 0.015 V the E_a increased for lithiation while decreasing for sodiation, as summarized in **Fig. 9**. We can regard values of E_a during the insertion process obtained from τ of chronocoulogram, $D_{app,later}$ estimated from PSCA, and R_{ct} evaluated by EIS are representing the entire reaction in slope/plateau region, the solid-state diffusion, and the charge-transfer, respectively. Evaluating E_a of Na insertion using R_{ct} provided similar results to thatobtained from τ in **Eq. 4** for the slope region from 1.0 V to 0.1 V. On the other hand, E_a increased in the middle of the plateau at 0.06 V. Finally, these E_a were converged to same order in E_a of $D_{app,later}$ at 0.015 V at the end of the plateau (**Fig. 9a**). This result implies that the plateau region accompanying pseudo-metallic cluster formation becomes the rate-determining step of full sodiation of HC. Furthermore, it can suppress the kinetics of other elemental reactions, i.e., desolvation and diffusion of sodium ions/atoms in pseudo graphitic-layer[40] during propagation of cluster into inner-pores like core-shell model,[15] as illustrated in reaction coordination. On the other hand, greater E_a attributed to τ and R_{ct} for Li insertion was observed even in the lowest potential implying that the higher energy for Li clustering can limit Li-insertion rate in plateau region, and there might be homogeneous filling into inner-pore not following the core-shell model.

In total, our various results indicate sodium insertion into this HC is faster than lithium. Here the origin of this advantage of sodiation is speculated as follows: i) weak interaction between sodium atoms and defects in graphene sheet, ii) less sodium atom occupancy in the interlayer space, and iii) less nucleation energy of the pseudo-metal clustering within the nanopores. For point i), DFT calculations indicate that lithium has stronger interactions with carbon than sodium.[24,64–66] The HC used in this study also contains sulfur at elemental compositions of ~1 wt.% as shown in Fig. S2c, which may form sulfur-containing defects in the graphitic interlayers. Like carbon, these sulfur defects may show weaker interactions with sodium that enable easier sodium ion migration at the vicinity of the defects compared with lithium.[67] For point ii), according to reports revealing the storage site, less sodium is stored in interlayer space of HC compared with Li^+.[2,66] The reported selectiveness of this storage site in HCs may enhance sodium diffusion and prevent trapping. Finally, for point iii), Li et al.,[24] Morita and Gotoh et al. [7,64] have reported that pseudo-metallic Na clusters are more energetically favorable in HCs with similar micropore size as our HC. In addition, Aniskevich et al. found that sodium diffusion includes transport from the interlayer to the pore that can limit the sodiation rate.[54] Our estimated activation energies obtained from temperature testing are consistent with these previous result.

Conclusions

In this study, we have used the diluted electrode method to deeply investigate the kinetics of sodiation and lithiation at HC. Based on charge/discharge testing, CV and PSCA under temperature control, the solid-state diffusion in HC is found to be faster than liquid-state transportation within the electrolyte found inside the composite electrode porous network. This leads to serious rate-limitations with inhomogeneous SOC across the composite electrode bulk. In diluted HC-electrodes, Na cells showed remarkably higher rate-performance than Li, where we could obtain 80 % and 40 % of the full capacity at rates of 1,000 and 2,500 mA $g_{(HC)}^{-1}$, respectively, with proper accessibility to the plateau region. For the Li case, we found less impact by using the dilute electrode method with rapid fading to ~60 % at low charging rates of 200 mA g^{-1}. However, the undiluted electrodes showed a good rate capability that remained > 40 % up to 1,000 mA g^{-1} for lithiation, which was improved over sodiation at the undiluted HC-electrode showing a capacity of only 40 % up ~100 mA $g_{(HC)}^{-1}$. This discretion is likely depending on the contribution of complex resistances associated to composite-electrodes structure as rate limiting. Overall, the rate capability of sodium insertion was determined to be faster and show less impedance compared with lithium insertion at the same HC, as well as comparable to the lithium intercalation into diluted graphite-electrodes. The estimated D_{app} and E_a for sodiation and lithiation showed differences in pseudo-metallic cluster nucleation during pore-filling, but similar Na^+- and Li^+-diffusion rates during adsorption and insertion into the interlayer. Our results suggest interesting capabilities for fast sodiation of HC can be investigated by the dilute electrode method and a core-shell model, which may be similar with high-capacity HCs as developed in our laboratory. Further studies relating to HC structure,[11] electrolyte, electrolyte additives, binder, and other alkali-metal ions i.e., K^+,[68] Rb^+,[69] and Cs^+[70], furthermore, alloys,[71] layered oxides, polyanion compounds, and Prussian blue analogues[34,63,72] are currently ongoing.

Author contributions

Y. F.: Conceptualization, Investigation, Writing – original draft; Z. T. G. and R. T.: Investigation, Writing – review & editing; S. K.: Supervision, Investigation, Writing – review & editing.

Conflicts of interest

The authors declare no competing interests.

Data availability

The datasets in the current study are available from the corresponding author on reasonable request.

Acknowledgements

The authors gratefully appreciate Rena Takaishi and Takashi Matsuyama in NIPPON A&L INC. for their fruitful discussion, and Assoc. prof. Kingo Ariyoshi in Osaka Metropolitan University for

his instruction and discussion about the diluted-electrode method. Y.F. thanks Ms. Ayame Sasaki and Mr. Tadanori Kawamata for their experimental support, and Dr. Daisuke Igarashi and Dr. Tomooki Hosaka for their assistance in manuscript preparation. This study was partially funded by the Ministry of Education, Culture, Sports, Science and Technology (MEXT) Program: Data Creation and Utilization Type Materials Research. (JPMXP1122712807), the JST through CREST (Grant No. JPMJCR21O6), ASPIRE (JPMJAP2313), and GteX (JPMJGX23S4), and JSPS-Grant-in-Aid for JSPS Fellows (24KJ2024).

References

1 Z. T. Gossage, D. Igarashi, Y. Fujii, M. Kawaguchi, R. Tatara, K. Nakamoto and S. Komaba, *Chem. Sci.*, 2024, **15**, 18272–18294.
2 K. Kubota, S. Shimadzu, N. Yabuuchi, S. Tominaka, S. Shiraishi, M. Abreu-Sepulveda, A. Manivannan, K. Gotoh, M. Fukunishi, M. Dahbi and S. Komaba, *Chem. Mater.*, 2020, **32**, 2961–2977.
3 J. M. Stratford, A. K. Kleppe, D. S. Keeble, P. A. Chater, S. S. Meysami, C. J. Wright, J. Barker, M.-M. Titirici, P. K. Allan and C. P. Grey, *J. Am. Chem. Soc.*, 2021, **143**, 14274–14286.
4 H. Hijazi, Z. Ye, E. Zsoldos, M. Obialor, W. Black, S. Azam, J. R. Dahn and M. Metzger, *J. Electrochem. Soc.*, 2024, **171**, 050521.
5 D. Igarashi, Y. Tanaka, K. Kubota, R. Tatara, H. Maejima, T. Hosaka and S. Komaba, *Advanced Energy Materials*, 2023, **13**, 2302647.
6 Y. Morikawa, S. Nishimura, R. Hashimoto, M. Ohnuma and A. Yamada, *Advanced Energy Materials*, 2020, **10**, 1903176.
7 K. Gotoh, M. Maeda, A. Nagai, A. Goto, M. Tansho, K. Hashi, T. Shimizu and H. Ishida, *Journal of Power Sources*, 2006, **162**, 1322–1328.
8 C.-W. Tai, W.-Y. Jao, L.-C. Tseng, P.-C. Wang, A.-P. Tu and C.-C. Hu, *J. Mater. Chem. A*, 2023, **11**, 19669–19684.
9 N. Takami, A. Satoh, M. Hara and T. Ohsaki, *J. Electrochem. Soc.*, 1995, **142**, 371–379.
10 K. Gotoh, T. Yamakami, I. Nishimura, H. Kometani, H. Ando, K. Hashi, T. Shimizu and H. Ishida, *J. Mater. Chem. A*, 2020, **8**, 14472–14481.
11 Y. Fujii, H. Yoshimo, R. Tatara, Z. T. Gossage, A. Koizumi and S. Komaba, *ACS Appl. Energy Mater.*, 2025, **8**, 6577–6585.
12 Y. Orikasa, Y. Gogyo, H. Yamashige, M. Katayama, K. Chen, T. Mori, K. Yamamoto, T. Masese, Y. Inada, T. Ohta, Z. Siroma, S. Kato, H. Kinoshita, H. Arai, Z. Ogumi and Y. Uchimoto, *Sci Rep*, 2016, **6**, 26382.
13 K. Kitada, H. Murayama, K. Fukuda, H. Arai, Y. Uchimoto, Z. Ogumi and E. Matsubara, *Journal of Power Sources*, 2016, **301**, 11–17.
14 K. Dokko, N. Nakata, Y. Suzuki and K. Kanamura, *J. Phys. Chem. C*, 2010, **114**, 8646–8650.
15 N. Takami, K. Hoshina and H. Inagaki, *J. Electrochem. Soc.*, 2011, **158**, A725–A730.
16 J. Suzuki, N. Kubota, Y. Omura, K. Sugata, K. Kisa, H. Sofuji and M. Hattori, *Electrochemistry*, 2018, **86**, 116–121.
17 Y. Fujii, K. Sugata, Y. Omura, N. Kubota, K. Kisa, H. Sofuji and J. Suzuki, *Electrochemistry*, 2023, **91**, 077008–077008.
18 K. Ariyoshi, S. Mizutani, T. Makino and Y. Yamada, *J. Electrochem. Soc.*, 2018, **165**, A3965–A3970.
19 K. Ariyoshi, J. Sugawa and S. Masuda, *J. Electrochem. Soc.*, 2020, **167**, 140517.
20 K. Ariyoshi, J. Sugawa and S. Masuda, *Journal of Power Sources*, 2021, **509**, 230349.
21 K. Ariyoshi and J. Sugawa, *Electrochimica Acta*, 2023, **455**, 142425.
22 K. Ariyoshi and S. Hiroshima, *Electrochimica Acta*, 2024, **487**, 144192.
23 Y. Fujii, R. Tatara, D. Igarashi, T. Hosaka, R. Takaishi, E. Shiiyama, T. Matsuyama and S. Komaba, *Electrochemistry*, 2023, **91**, 077002–077002.
24 Y. Li, A. Vasileiadis, Q. Zhou, Y. Lu, Q. Meng, Y. Li, P. Ombrini, J. Zhao, Z. Chen, Y. Niu, X. Qi, F. Xie, R. van der Jagt, S. Ganapathy, M.-M. Titirici, H. Li, L. Chen, M. Wagemaker and Y.-S. Hu, *Nat Energy*, 2024, **9**, 134–142.
25 Kureha Battery Materials Japan Co., Ltd., "High-performance Anode Material CARBOTRON® P" https://www.kureha.co.jp/development/story/pdf/catalog_hc_eg_20120924.pdf, (accessed 2023/04/30).
26 FUJIFILM Wako Pure Chemical Corporation, "SAFETY DATA SHEET Aluminium Oxide" https://labchem-wako.fujifilm.com/sds/W01W0101-0196JGHEEN.pdf (accessed 2025/09/29).
27 International Chemical Safety Card, "POLYACRYLIC ACID, SODIUM SALT" https://www.ilo.org/dyn/icsc/showcard.display?p_card_id=1429&p_version=2&p_lang=en (accessed 2023/04/30).
28 H. Kondo, H. Sawada, C. Okuda and T. Sasaki, *J. Electrochem. Soc.*, 2019, **166**, A1285–A1290.
29 R. Tian, N. Alcala, S. J. K. O'Neill, D. V. Horvath, J. Coelho, A. J. Griffin, Y. Zhang, V. Nicolosi, C. O'Dwyer and J. N. Coleman, *ACS Appl. Energy Mater.*, 2020, **3**, 2966–2974.
30 T. Yamamoto, T. Yamaguchi, T. Nohira, R. Hagiwara, A. Fukunaga, S. Sakai and K. Nitta, *Electrochemistry*, 2017, **85**, 391–396.
31 S. Komaba, W. Murata, T. Ishikawa, N. Yabuuchi, T. Ozeki, T. Nakayama, A. Ogata, K. Gotoh and K. Fujiwara, *Adv Funct Materials*, 2011, **21**, 3859–3867.
32 H. Hijazi, Z. Ye, L. Zhang, J. Deshmukh, M. B. Johnson, J. R. Dahn and M. Metzger, *J. Electrochem. Soc.*, 2023, **170**, 070512.
33 J. Landesfeind, T. Hosaka, M. Graf, K. Kubota, S. Komaba and H. A. Gasteiger, *J. Electrochem. Soc.*, 2021, **168**, 040538.
34 E. J. Kim, P. R. Kumar, Z. T. Gossage, K. Kubota, T. Hosaka, R. Tatara and S. Komaba, *Chem. Sci.*, 2022, **13**, 6121–6158.
35 S. Tsujimoto, Y. Kondo, Y. Yokoyama, Y. Miyahara, K. Miyazaki and T. Abe, *J. Electrochem. Soc.*, 2021, **168**, 070508.
36 R. Mogensen, D. Brandell and R. Younesi, *ACS Energy Lett.*, 2016, **1**, 1173–1178.
37 T. Takamura, *Electrochemistry*, 2012, **80**, 3–14.
38 K. Ariyoshi and J. Sugawa, *Electrochemistry*, 2021, **89**, 157–161.
39 M. Okubo, Y. Tanaka, H. Zhou, T. Kudo and I. Honma, *J. Phys. Chem. B*, 2009, **113**, 2840–2847.
40 Y. Aniskevich, J. H. Yu, J. Kim, S. Komaba and S. Myung, *Advanced Energy Materials*, 2024, 2304300.
41 Z. Guo, Z. Xu, F. Xie, J. Jiang, K. Zheng, S. Alabidun, M. Crespo-Ribadeneyra, Y. Hu, H. Au and M. Titirici, *Advanced Materials*, 2023, **35**, 2304091.
42 D. Ledwoch, L. Komsiyska, E.-M. Hammer, K. Smith, P. R. Shearing, D. J. L. Brett and E. Kendrick, *Electrochimica Acta*, 2022, **401**, 139481.
43 K. Ando, M. Tsuta and K. Kanamura, *Journal of Electroanalytical Chemistry*, 2023, **948**, 117802.
44 S. R. Narayanan, D. H. Shen, S. Surampudi, A. I. Attia and G. Halpert, *J. Electrochem. Soc.*, 1993, **140**, 1854–1861.
45 N. Takami, A. Satoh, M. Hara and T. Ohsaki, *J. Electrochem. Soc.*, 1995, **142**, 371–379.
46 R. Dong, L. Zheng, Y. Bai, Q. Ni, Y. Li, F. Wu, H. Ren and C. Wu, *Advanced Materials*, 2021, **33**, 2008810.
47 X. Yi, X. Li, J. Zhong, S. Wang, Z. Wang, H. Guo, J. Wang and G. Yan, *Adv Funct Materials*, 2022, 2209523.
48 M. Nishizawa, *Electrochem. Solid-State Lett.*, 1999, **1**, 10.
49 M. Nishizawa, H. Koshika, R. Hashitani, T. Itoh, T. Abe and I. Uchida, *J. Phys. Chem. B*, 1999, **103**, 4933–4936.
50 K. Dokko, M. Mohamedi, M. Umeda and I. Uchida, *Journal of The Electrochemical Society*.
51 K. Ohishi, D. Igarashi, R. Tatara, S. Nishimura, A. Koda, S. Komaba and J. Sugiyama, *ACS Phys. Chem Au*, 2022, **2**, 98–107.
52 I. Umegaki, S. Kawauchi, H. Sawada, H. Nozaki, Y. Higuchi, K. Miwa, Y. Kondo, M. Månsson, M. Telling, F. C. Coomer, S. P. Cottrell, T. Sasaki, T. Kobayashi and J. Sugiyama, *Phys. Chem. Chem. Phys.*, 2017, **19**, 19058–19066.
53 S. Yang, B. Yan, J. Wu, L. Lu and K. Zeng, *ACS Appl. Mater. Interfaces*, 2017, **9**, 13999–14005.
54 Y. Aniskevich, J. H. Yu, J. Kim, S. Komaba and S. Myung, *Advanced Energy Materials*, 2024, 2304300.
55 G. Hasegawa, K. Kanamori, N. Kannari, J. Ozaki, K. Nakanishi and T. Abe, *Journal of Power Sources*, 2016, **318**, 41–48.
56 F. Linsenmann, D. Pritzl and H. A. Gasteiger, *J. Electrochem. Soc.*, 2021, **168**, 010506.
57 K. Ariyoshi, S. Mizutani and Y. Yamada, *Journal of Power Sources*, 2019, **435**, 226810.

View Article Online
DOI: 10.1039/D5SC07762A

58 K. Ariyoshi, M. Tanimoto and Y. Yamada, *Electrochimica Acta*, 2020, **364**, 137292.
59 H. Nara, K. Morita, D. Mukoyama, T. Yokoshima, T. Momma and T. Osaka, *Electrochimica Acta*, 2017, **241**, 323–330.
60 E. Barsoukov, J. H. Kim, J. H. Kim, C. O. Yoon and H. Lee, *Solid State Ionics*, 1999, **116**, 249–261.
61 H. Nara, D. Mukoyama, T. Yokoshima, T. Momma and T. Osaka, *J. Electrochem. Soc.*, 2016, **163**, A434–A441.
62 H. Kim, S. K. Oh, J. Lee, S. W. Doo, Y. Kim and K. T. Lee, *Electrochimica Acta*, 2021, **370**, 137743.
63 T. Hosaka, K. Kubota, A. S. Hameed and S. Komaba, *Chem. Rev.*, 2020, **120**, 6358–6466.
64 R. Morita, K. Gotoh, M. Fukunishi, K. Kubota, S. Komaba, N. Nishimura, T. Yumura, K. Deguchi, S. Ohki, T. Shimizu and H. Ishida, *J. Mater. Chem. A*, 2016, **4**, 13183–13193.
65 Q. Li, J. Zhang, L. Zhong, F. Geng, Y. Tao, C. Geng, S. Li, B. Hu and Q. Yang, *Advanced Energy Materials*, 2022, **12**, 2201734.
66 H. Kim, J. C. Hyun, D.-H. Kim, J. H. Kwak, J. B. Lee, J. H. Moon, J. Choi, H.-D. Lim, S. J. Yang, H. M. Jin, D. J. Ahn, K. Kang, H.-J. Jin, H.-K. Lim and Y. S. Yun, *Advanced Materials*, 2023, **35**, 2209128.
67 E. Olsson, G. Chai, M. Dove and Q. Cai, *Nanoscale*, 2019, **11**, 5274–5284.
68 S. Komaba, T. Hasegawa, M. Dahbi and K. Kubota, *Electrochemistry Communications*, 2015, **60**, 172–175.
69 D. Igarashi, R. Tatara, R. Fujimoto, T. Hosaka and S. Komaba, *Chem. Sci.*, 2023, **14**, 11056–11066.
70 A. Yadav, H. Kobayashi, T. Yamamoto and T. Nohira, *Electrochemistry*, 2024, **92**, 043008–043008.
71 S. Yamazaki, R. Tatara, H. Mizuta, K. Kawano, S. Yasuno and S. Komaba, *Mater. Adv.*, 2023, **4**, 1637–1647.
72 N. Yabuuchi, K. Kubota, M. Dahbi and S. Komaba, *Chem. Rev.*, 2014, **114**, 11636–11682.

View Article Online
DOI: 10.1039/D5SC07762A

Data availability

The datasets in the current study are available from the corresponding author on reasonable request.